



# Neutrino quantum kinetics in three flavors

**Shashank Shalgar**  <sup>a</sup> and **Irene Tamborra**  <sup>a</sup>

<sup>a</sup>Niels Bohr International Academy & DARK, Niels Bohr Institute,  
University of Copenhagen, Blegdamsvej 17, 2100 Copenhagen, Denmark

E-mail: [shashank.shalgar@nbi.ku.dk](mailto:shashank.shalgar@nbi.ku.dk), [tamborra@nbi.ku.dk](mailto:tamborra@nbi.ku.dk)

**Abstract.** The impact of neutrino flavor conversion on the supernova mechanism is yet to be fully understood. We present multi-energy and multi-angle solutions of the neutrino quantum kinetic equations in three flavors, taking into account neutrino advection and non-forward collisions with the background medium. Flavor evolution is explored within a spherically symmetric shell surrounding the region of neutrino decoupling in the interior of a core-collapse supernova, relying on the outputs of a spherically symmetric core-collapse supernova model with a mass of  $18.6M_{\odot}$ . We select two representative post-bounce times:  $t_{\text{pb}} = 0.25$  s (no angular crossings are present and flavor conversion is triggered by slow collective effects) and  $t_{\text{pb}} = 1$  s (angular crossings trigger fast flavor instabilities). We find that flavor equipartition is achieved in the antineutrino sector between  $\bar{\nu}_e$  and  $\bar{\nu}_x = (\bar{\nu}_{\mu} + \bar{\nu}_{\tau})/2$  for both post-bounce times. In the neutrino sector, flavor equipartition between  $\nu_e$  and  $\nu_x$  seems more likely at later post-bounce times, where the neutrino emission properties among different flavors tend to approach each other, but it is not a generic feature. The exponential growth of the  $\nu_{\mu}-\nu_{\tau}$  asymmetry due to three-flavor effects is responsible for differences between the quasi-steady configurations obtained in the three-flavor solution and in the two-flavor approximation. This has consequences on the neutrino heating rate, which is generally larger when all three flavors are taken into account and can increase up to 30% with respect to the case where flavor conversion is neglected.

---

## Contents

<b>1</b>	<b>Introduction</b>	<b>1</b>
<b>2</b>	<b>Neutrino equations of motion</b>	<b>2</b>
<b>3</b>	<b>Problem setup</b>	<b>3</b>
<b>4</b>	<b>Flavor evolution in three flavors</b>	<b>5</b>
4.1	Quasi-steady-state flavor configuration	5
4.2	Growth of the off-diagonal elements of the density matrix	5
4.3	Three-flavor features of the neutrino distributions in energy and angle	6
<b>5</b>	<b>Crossings in the muon- and tau-lepton-number distributions</b>	<b>7</b>
<b>6</b>	<b>Heating rate</b>	<b>8</b>
<b>7</b>	<b>Conclusions</b>	<b>10</b>
<b>A</b>	<b>Matter background and neutrino self-interaction</b>	<b>12</b>
A.1	Neutrino bulb model	13
A.2	Matter effects on flavor transformation in the quantum kinetic approach	14
<b>B</b>	<b>Are neutrinos emitted as flavor eigenstates in the interior of a core-collapse supernova?</b>	<b>15</b>

---

## 1 Introduction

Neutrino flavor evolution in dense astrophysical environments, such as core-collapse supernovae and neutron-star mergers, is driven by the refraction experienced by neutrinos when passing through a medium of electrons as well as other neutrinos [1–4]. However, unlike neutrino refraction off electrons, neutrino-neutrino self-interaction is a non-linear phenomenon that depends on the neutrino flavor evolving dynamically [5–8].

Favorable conditions for flavor conversion can be present in the neutrino decoupling region of core-collapse supernovae and neutron-star mergers, with possible implications on the explosion mechanism and nucleosynthesis [9–16]. In particular, while decoupling, neutrinos can undergo fast flavor conversion in the limit of vanishing vacuum frequency (or equivalently for large neutrino number density) [17–21]. Fast conversion is possible, if a crossing in the lepton number angular distribution of neutrinos exists [20–23]. In the absence of crossings, the time-scale characterizing collective flavor conversion is longer and defined by a combination of the vacuum oscillation frequency and the neutrino self-interaction strength (slow collective flavor conversion) [24–30]. Due to the non-trivial angular distributions of neutrinos in the decoupling region, fast flavor conversion can also be seeded by slow collective effects, leading to an effective crossing in the angular distribution of the neutrino lepton number [31, 32]. Although, the time-scale associated with flavor evolution is shorter than the ones characterizing neutrino advection and non-forward collisions with the background medium, the latter do affect flavor conversion [30, 33–40].

The numerical solution of the neutrino quantum transport is challenged by the vast gradient of scales entering the problem. Therefore, in order to make the problem tractable, several approximations and/or symmetry assumptions have been employed. One of these being the investigation of neutrino conversion physics in the two-flavor approximation. This simplification was justified because 1. the atmospheric mass difference,  $\Delta m^2$ , is larger than the solar one,  $\delta m^2$ , by a factor of  $\mathcal{O}(30)$ —and both are much smaller of the neutrino self-interaction strength  $\mu \sim \sqrt{2}G_F n_\nu$ , with  $G_F$  being the Fermi constant and  $n_\nu$  the neutrino number density; 2. the temperature in the core of supernovae is such that the emission properties of  $\nu_\mu$  and  $\nu_\tau$  can be approximately assumed to be indistinguishable [24, 28]. In the context of slow collective flavor evolution, the two-flavor approximation was deemed to be a good approximation of the final flavor outcome [41–46]. However, in the context of fast flavor conversion, the off-diagonal component of the density matrix  $\rho_{\mu\tau}$  grows faster than  $\rho_{e\tau}$  and  $\rho_{e\mu}$  in homogenous systems, leading to a different final flavor configuration with respect to the one obtained in the two-flavor solution [47, 48].

Recent core-collapse supernova and neutron-star-merger simulations show that muon production could take place in the source core, leading to different distributions between the  $\mu$  and  $\tau$  neutrino flavors [49–52]. This finding, together with the fact that the angular distributions of the non-electron flavors may also develop crossings [53] and that flavor instabilities linked to three flavor effects can largely affect the flavor outcome [38, 47, 48, 54–57], calls for an investigation of the neutrino quantum kinetics in three flavors. In this paper, we do so by expanding our multi-angle and multi-energy solution of the neutrino quantum kinetic equations in two flavors [32]. We assume identical  $\nu_\mu$  and  $\nu_\tau$  distributions in the absence of flavor conversion and solve the equations of motion of neutrinos in a spherically symmetric shell embedding the region of neutrino decoupling, relying on inputs from a one-dimensional core-collapse supernova model with a mass of  $18.6 M_\odot$  [58]. Our goal is to identify differences in the  $\nu_\mu$ – $\nu_\tau$  sector due to flavor conversion.

This paper is organized as follows. In Sec. 2, the neutrino equations of motion in three flavors are introduced. Section 3 outlines the method adopted to solve the neutrino equations of motion adopting the thermodynamic and hydrodynamic properties of selected post-bounce times of our benchmark supernova model. We present our findings on flavor evolution in three flavors in Sec. 4. The impact of crossings in the angular distribution of the muon- and tau-neutrino lepton numbers is discussed in Sec. 5, while we quantify the feedback of three-flavor effects on the supernova heating rate in Sec. 6. Finally, we summarize our findings in Sec. 7. In addition, we explore whether it is justified to neglect the matter term in lieu of effective mixing angles in Appendix A. Appendix B investigates if the quasi-steady-state flavor configuration is affected by neutrinos being emitted as mixed flavor eigenstates.

## 2 Neutrino equations of motion

The flavor states for neutrinos and antineutrinos can be described relying on the density matrices,  $\rho(\cos\theta, E, r, t)$  and  $\bar{\rho}(\cos\theta, E, r, t)$ , that are functions of the neutrino emission angle ( $\cos\theta$ ), propagation radius ( $r$ ), energy ( $E$ ), and time ( $t$ ), respectively. The diagonal components of the density matrices represent the occupation numbers of the flavor states, while the off-diagonal components take into account the coherence between the flavor states.

The neutrino flavor evolution is described by the following equations [59]:

$$i \left( \frac{\partial}{\partial t} + \vec{v} \cdot \nabla \right) \rho(\cos \theta, E, r, t) = [H(\cos \theta, E, r, t), \rho(\cos \theta, E, r, t)] + i\mathcal{C}[\rho, \bar{\rho}] , \quad (2.1)$$

$$i \left( \frac{\partial}{\partial t} + \vec{v} \cdot \nabla \right) \bar{\rho}(\cos \theta, E, r, t) = [\bar{H}(\cos \theta, E, r, t), \bar{\rho}(\cos \theta, E, r, t)] + i\bar{\mathcal{C}}[\rho, \bar{\rho}] . \quad (2.2)$$

On the left hand side of Eqs. 2.1 and 2.2, the term  $\vec{v} \cdot \nabla = \cos \theta \partial / \partial r + (\sin^2 \theta / r)(\partial / \partial \cos \theta)$  takes into account the motion of (anti)neutrinos; note that  $r$  and  $t$  are not interchangeable in Eqs. 2.1 and 2.2 in the presence of inhomogeneities.

On the right hand side of Eqs. 2.1 and 2.2, the commutator encapsulates all the physics linked to flavor conversion. The Hamiltonian contains the vacuum, matter, and self-interaction terms:

$$H(\cos \theta, E, r, t) = H_{\text{vac}}(E) + H_{\text{mat}}(r, t) + H_{\nu\nu}(\cos \theta, r, t) , \quad (2.3)$$

$$\bar{H}(\cos \theta, E, r, t) = -H_{\text{vac}}(E) + H_{\text{mat}}(r, t) + H_{\nu\nu}(\cos \theta, r, t) . \quad (2.4)$$

Each of these terms is defined as

$$H_{\text{vac}} = U_{\text{PMNS}} \frac{\text{diag}(M^2)}{2E} U_{\text{PMNS}}^\dagger , \quad (2.5)$$

$$H_{\text{mat}} = \text{diag}(\lambda(r), 0, 0) , \quad (2.6)$$

$$H_{\nu\nu} = \xi \int_{-1}^1 d \cos \theta' \int_0^\infty dE [\rho(\cos \theta', E, r, t) - \bar{\rho}(\cos \theta', E, r, t)] \times (1 - \cos \theta \cos \theta') . \quad (2.7)$$

In  $H_{\text{vac}}$ , the diagonal matrix  $M^2$  is a function of the squared neutrino mass differences ( $\delta m^2$  and  $\Delta m^2$ ) and  $U_{\text{PMNS}}(\vartheta_V^{12}, \vartheta_V^{13}, \vartheta_V^{23}, \delta_{\mathcal{CP}})$  is the  $3 \times 3$  Pontecorvo–Maki–Nakagawa–Sakata mixing matrix, which is a function of the three neutrino mixing angles and the  $\mathcal{CP}$ -violation phase. In  $H_{\text{mat}}$ ,  $\lambda(r) = \sqrt{2} G_{\text{F}} n_e(r)$  is the matter potential with  $n_e$  being the number density of electrons. The neutrino self-interaction Hamiltonian is given by  $H_{\nu\nu}$ ; in order to facilitate the numerical solution of Eqs. 2.1 and 2.2, we introduce an attenuation factor  $\xi$  in  $H_{\nu\nu}$  following Ref. [35].

The collision terms appearing on the right hand side of Eqs. 2.1 and 2.2 include the emission, absorption, and the direction-changing non-forward scattering terms [59, 60]:

$$\begin{aligned} \mathcal{C} &= \mathcal{C}^{\text{emit}}(E, r) - \mathcal{C}^{\text{absorb}}(E, r) \rho(\cos \theta, E, r, t) \\ &\quad - \mathcal{C}^{\text{dir-ch}}(E, r) \rho(\cos \theta, E, r, t) + \frac{\mathcal{C}^{\text{dir-ch}}}{2}(r, E) \int_{-1}^1 \rho(\cos \theta', E, r, t) d \cos \theta' \\ &\quad + \cos \theta \mathcal{C}^{\text{ani}}(r, E) \int_{-1}^1 d \cos \theta' \cos \theta' \rho(\cos \theta', E, r, t) . \end{aligned} \quad (2.8)$$

### 3 Problem setup

In the following, unless otherwise specified, we neglect the matter term and instead use small mixing angles of  $\vartheta_V^{12} = \vartheta_V^{13} = \vartheta_V^{23} = 10^{-3}$ ; we refer the interested reader to Appendix A for a proof of the validity of such a choice. Moreover, we assume  $\delta_{\mathcal{CP}} = 0$  for the sake of simplicity and  $\delta m^2 = 7.5 \times 10^{-5} \text{ eV}^2$  and  $\Delta m^2 = 2.5 \times 10^{-3} \text{ eV}^2$  [61]. We attenuate the strength of the neutrino self-interaction strength by a factor  $\xi = 10^{-2}$ .

The effective mixing angles are the only source of initial perturbation in the off-diagonal components of the Hamiltonian. The suppression of the mixing angle due to matter effects is possible only if neutrinos are emitted in flavor eigenstates, but the (anti)neutrino density matrices can have non-zero off-diagonal components at production in the core of a supernova because of neutral-current interactions, such as pair-production and Bremsstrahlung. Nevertheless, as shown in Appendix B, the correction of the off-diagonal components of the density matrix is negligible with respect to the off-diagonal terms generated by the matter term.

The neutrino flavor evolution depends on the thermodynamic and hydrodynamic properties of the source, which enter the collision terms. We adopt a static hydrodynamic background and thermodynamical properties for selected post-bounce times of a one-dimensional hydrodynamic core-collapse supernova simulation. Our benchmark supernova model has a progenitor mass of  $18.6M_{\odot}$ , gravitational mass of  $1.4M_{\odot}$ , and SFHo equation of state [58]. This supernova model does not include muons and the effect of proto-neutron star convection is taken into account through a mixing-length approximation. The energy-dependent collision terms have been implemented as in Ref. [32] (see also Appendix A of Ref. [62]). We stress that we assume the distributions of  $\nu_{\mu}$ 's and  $\nu_{\tau}$ 's to be identical in the absence of flavor conversion and determined by pair production and Bremsstrahlung.

In what follows, we consider two representative post-bounce times:  $t_{\text{pb}} = 0.25$  s and  $t_{\text{pb}} = 1$  s. These two times have been chosen since no electron lepton number (ELN) crossing appears for  $t_{\text{pb}} = 0.25$  s and therefore flavor conversion is triggered by slow collective effects; for  $t_{\text{pb}} = 1$  s, an ELN crossing is instead present and flavor conversion is driven by the fast flavor instability. We solved the quantum kinetic equations for  $t_{\text{pb}} = 0.05, 0.12, 0.25, 0.5, 0.75,$  and  $1$  s; for all configurations corresponding to  $t_{\text{pb}} \gtrsim 0.5$  s, we find an ELN crossing and the final flavor configuration has a behavior qualitatively similar to the one obtained for  $t_{\text{pb}} = 1$  s (results not shown here).

Equations 2.1 and 2.2 suggest that, in order to investigate neutrino flavor evolution, we need to solve a boundary problem. To do so, we discretize the density matrices over the energy, the polar angle, and the radial range: we use 25 energy bins in the range between 0 and 50 MeV, 75 angle bins, and 150 radial bins. The cosine of the polar angle ( $\cos \theta$ ) ranges between  $-1$  and  $1$ , corresponding to neutrinos traveling in radially backward and forward directions, respectively. Since neutrino decoupling is not instantaneous, but occurs gradually in an extended spatial region [63, 64], we track the neutrino flavor evolution in a radial range such that neutrinos of all flavors are in thermal equilibrium at the smallest radius ( $r_{\text{min}}$ ) and all flavors free-stream at the largest radius ( $r_{\text{max}}$ ). In order to ensure that neutrinos have a Fermi-Dirac distribution at  $r_{\text{min}}$  and there is no flux in the backward direction at  $r_{\text{max}}$ , we solve the quantum kinetic equations in the radial range of [22, 57] km for  $t_{\text{pb}} = 0.25$  s and we consider [16, 31] km for  $t_{\text{pb}} = 1$  s.

The temporal evolution of the equations of motion is carried out using an adaptive step-size with absolute and relative tolerances of  $10^{-6}$ . The advective term in the equations of motion involves a derivative with respect to the polar angle and the radius; we perform such derivative by using the central difference method. We refer the reader to Refs. [32, 65, 66] for additional details on the setup of the numerical simulations.

Following the approach introduced in Refs. [65, 66]. First we assume  $H = \bar{H} = 0$  and evolve the system until the neutrino flavor configuration reaches a steady state (classical-steady state). Then, taking into account flavor conversion, the system is further evolved until a quasi-steady-state configuration is achieved (i.e., we solve Eqs. 2.1 and 2.2 until the

diagonal components of the density matrices become independent of time, except for some numerical fluctuations; note that the off-diagonal components of the density matrices never reach this state).

## 4 Flavor evolution in three flavors

In this section, we characterize the quasi-steady-state flavor configuration obtained as a consequence of flavor conversion. In order to do that, we explore the growth of the off-diagonal elements of the density matrix, as well as the distributions of neutrinos and antineutrinos in angle and energy obtained by taking into account flavor conversion.

### 4.1 Quasi-steady-state flavor configuration

The left panels of Fig. 1 represent the heatmap of the distribution of  $\rho_{ee} - \bar{\rho}_{ee}$  in the plane spanned by  $\cos\theta$  and  $r$  for  $t_{\text{pb}} = 0.25$  s (top) and 1 s (bottom) in the absence of neutrino flavor conversion (classical-steady state). As already discussed in Ref. [32], for  $t_{\text{pb}} = 0.25$  s no crossing is present, as signified by the absence of blue colored regions in the heatmap; while the classical-steady-state configuration of  $t_{\text{pb}} = 1$  s has crossings in the transition region between the red and blue areas.

The right panels of Fig. 1 represent the quasi-steady-state configuration of  $\rho_{ee} - \bar{\rho}_{ee}$  after the three-flavor equations of motion have been evolved for  $t = 2 \times 10^{-4}$  s. In agreement with the two-flavor analog solution presented in Ref. [32], significant flavor evolution takes place due to the vacuum term that triggers neutrino self-interactions (slow collective flavor conversion) for the  $t_{\text{pb}} = 0.25$  s snapshot. On the other hand, for  $t_{\text{pb}} = 1$  s, flavor conversion develops near the crossing in the  $\rho_{ee} - \bar{\rho}_{ee}$  angular distribution (ELN crossing). However, it should be noted that the flavor instability is present only for a small radial region around 20–22 km for  $t_{\text{pb}} = 1$  s (cf. Sec. 4.2 and Fig. 2). The region beyond  $\approx 22$  km displays flavor conversion due to the advection of neutrinos that have undergone flavor evolution at smaller radii.

### 4.2 Growth of the off-diagonal elements of the density matrix

In order to investigate the role of the third flavor in the flavor evolution, we inspect the temporal evolution of the absolute values of the off-diagonal terms of the density matrices, after energy and angle integration. Figure 2 shows the temporal evolution of the off-diagonal terms at selected representative radii falling in the flavor instability region for  $t_{\text{pb}} = 0.25$  s (left panel) and  $t_{\text{pb}} = 1$  s (right panel). For  $t_{\text{pb}} = 0.25$  s, due to the absence of an ELN crossing, flavor conversion is triggered by the vacuum mixing terms (see also Fig. 6 of Ref. [62]). As a consequence, the growth rate of the off-diagonal terms is slower and it takes longer time to reach the non-linear regime. On the other hand, the temporal evolution of the off-diagonal terms of the density matrices for  $t_{\text{pb}} = 1$  s is driven by the development of the fast instability in the proximity of the ELN crossing. Interestingly, in this case we qualitatively find the same trend observed in the three-flavor studies for homogeneous systems [47, 48]: the off-diagonal component  $\rho_{\mu\tau}$  grows faster than  $\rho_{e\tau}$  and  $\rho_{e\mu}$ . The exponential growth of  $|\rho_{e\mu} - \rho_{e\tau}|$  (which does not occur in the two-flavor approximation) is responsible for breaking the symmetry between the  $\nu_\mu$  and  $\nu_\tau$  sectors [48]. Note that, even if  $\rho_{e\mu}$  and  $\rho_{e\tau}$  exhibit comparable growth rate, they are seeded by different initial perturbations because of the differences in the related vacuum terms of the Hamiltonian.

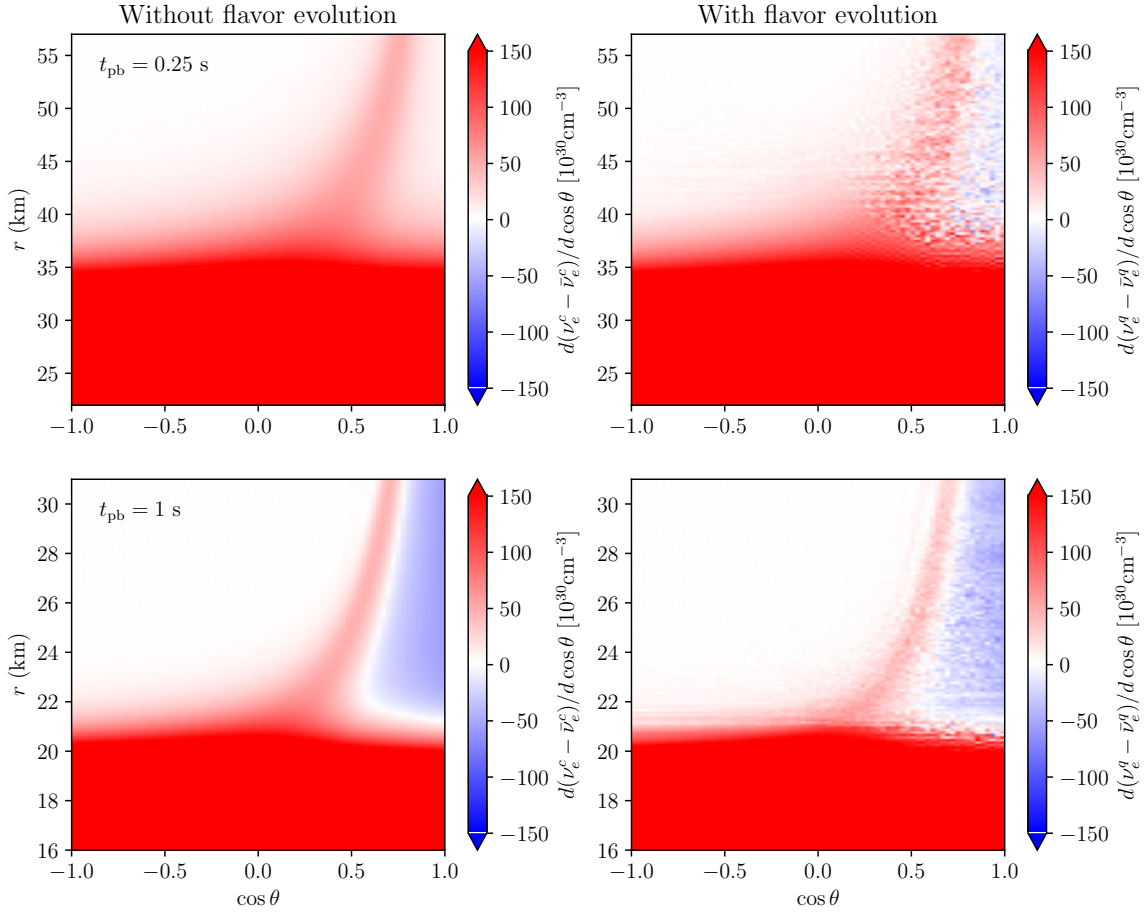


**Figure 1.** Heatmap of  $\rho_{ee} - \bar{\rho}_{ee}$  in the plane spanned by  $\cos \theta$  and  $r$  in the absence of flavor evolution (left panels, classical-steady state) and taking into account flavor evolution (right panels, quasi-steady state) for  $t_{\text{pb}} = 0.25$  s (top panels) and  $t_{\text{pb}} = 1$  s (bottom panels). For  $t_{\text{pb}} = 0.25$  s, ELN crossings are not present. Yet, flavor conversion develops triggered by the vacuum terms. For  $t_{\text{pb}} = 1$  s, ELN crossings develop in the classical-steady-state configuration, with resultant flavor conversion occurring in their proximity.

### 4.3 Three-flavor features of the neutrino distributions in energy and angle

The differences between the growth rates between the  $\nu_\mu$  and  $\nu_\tau$  sectors propagate into the non-linear phase. Figure 3 represents the quasi-steady-state energy distributions obtained for  $t_{\text{pb}} = 0.25$  s (top panels) and 1 s (bottom panels) for neutrinos on the left and antineutrinos on the right. We find that, for both time snapshots, flavor equipartition is achieved in the antineutrino sector in the sense that the energy spectrum for  $\bar{\nu}_e$  becomes comparable with that of  $\bar{\nu}_x = (\bar{\nu}_\mu + \bar{\nu}_\tau)/2$ . The same is true in the neutrino sector for  $t_{\text{pb}} = 1$  s, but not for  $t_{\text{pb}} = 0.25$  s. This is due to the fact that, at late post-bounce times, the neutrino distributions of all flavors tend to approach each other; this, in conjunction with the fact that neutrino self-interactions conserve the lepton number, implies that flavor equipartition in the neutrino and antineutrino sectors can be obtained with good approximation. However, this is not possible at earlier post-bounce times, where a larger difference among the neutrino emission properties of all flavors exists. It should be noted that, lepton number conservation



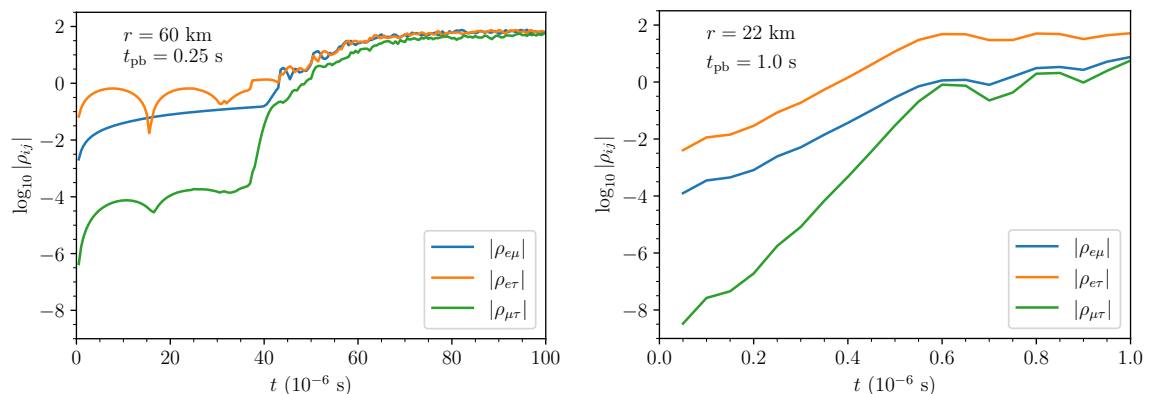


**Figure 2.** Temporal evolution of the off-diagonal components of the density matrix ( $\rho_{e\mu}$ ,  $\rho_{e\tau}$ , and  $\rho_{\mu\tau}$ ) as functions of time for  $t_{\text{pb}} = 0.25$  s and  $r = 60$  km (left panel)  $t_{\text{pb}} = 1$  s at  $r = 22$  km (right panel). The fast growth of  $|\rho_{e\mu} - \rho_{e\tau}|$  is responsible for breaking the symmetry between the  $\nu_\mu$  and  $\nu_\tau$  sectors with fast conversion being triggered by the ELN crossings for  $t_{\text{pb}} = 1$  s. A slower growth rate is observed for  $t_{\text{pb}} = 0.25$  s because the flavor instability is slow and the difference between the  $\mu$  and  $\tau$  sectors is purely due to the related vacuum terms in the Hamiltonian. Note that the  $x$ -scale of the left panel is smaller than the one of the right panel to highlight the growth of the fast flavor instability.

is not ensured in the numerical solution of the equations of motion because of the collision term. However, we do not find any significant lepton number violation for our benchmark configurations.

It is worth noticing that the survival probability in the antineutrino sector is  $\sim 1/3$  in the three-flavor scenario when flavor equipartition is achieved (see Fig. 3), while it is  $\sim 1/2$  in the two-flavor case. Figure 3 cannot be directly compared with the two-flavor solution presented in Figs. 8 and 9 of Ref. [32] since a different value of  $\xi$  was adopted in Ref. [32]; we find that significant flavor evolution occurs for  $\xi = 10^{-2}$  in the two-flavor approximation (results not shown here).

Figure 4 represents the angular distributions associated to the energy spectra in Fig. 3. For  $t_{\text{pb}} = 0.25$  s, once the quasi-steady-state configuration is achieved, the angular distributions of all three antineutrino flavors tend to approach each other; as for neutrinos, while the angular distributions of  $\nu_\mu$  and  $\nu_\tau$  are comparable, there is a slight excess of  $\nu_e$  over the other flavors. On the other hand, except for small differences, the angular distributions of all flavors of neutrinos and antineutrinos approach each other for  $t_{\text{pb}} = 1$  s.

## 5 Crossings in the muon- and tau-lepton-number distributions

Reference [49] pointed out that the large electron chemical potentials and high temperatures characteristic of the proto-neutron star can lead to the creation of muons. The latter could aid neutrino-driven explosions and favor the formation of angular crossings in the muon sector. Inspecting spherically-symmetric core-collapse supernova simulations with and without muons, Ref. [53] reported the existence of instabilities in the  $\mu$ - $\tau$  sector due to angular crossings.

Motivated by these findings, we modify our collision term to take into account the weak-magnetism corrections following the recipe presented in Ref. [67] (note that our supernova



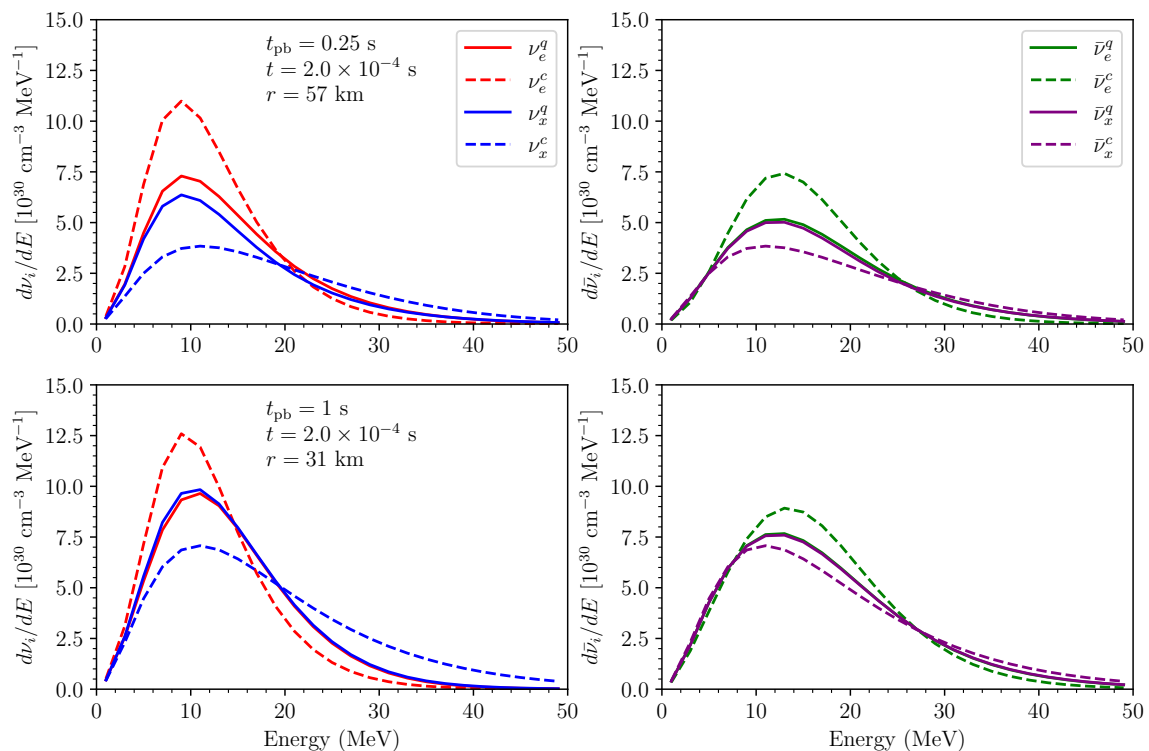


**Figure 3.** Energy spectra for  $\nu_e$  (red) and  $\nu_x$  (blue; with  $\nu_x = (\nu_\mu + \nu_\tau)/2$ ) in the left panels and  $\bar{\nu}_e$  (green) and  $\bar{\nu}(x)$  (purple; with  $\bar{\nu}_x = (\bar{\nu}_\mu + \bar{\nu}_\tau)/2$ ) in the right panels for  $t_{\text{pb}} = 0.25$  s on top and  $t_{\text{pb}} = 1$  s on the bottom. The energy spectra in the classical-steady-state (quasi-steady-state) configurations are shown as dashed (solid) lines. The quasi-steady-state distributions have been extracted at 57 km (31 km) after tracking the flavor evolution for  $2 \times 10^{-4}$  s for  $t_{\text{pb}} = 0.25$  s ( $t_{\text{pb}} = 1$  s). Equipartition is achieved in the antineutrino sector for  $t_{\text{pb}} = 0.25$  s, and both in the neutrino and antineutrino sectors for  $t_{\text{pb}} = 1$  s.

model does not include muons, therefore we do not take into account muon beta reactions). For the post-bounce profiles that we have investigated, we find that the collision term is larger for electron flavors due to beta reactions and therefore the angular distributions are negligibly affected by the weak magnetism corrections; however, crossings in the muon- and tau-flavor lepton numbers arise due to differences in  $\mathcal{C}_{\text{dir-ch}}$  for  $\nu_{\mu/\tau}$  and  $\bar{\nu}_{\mu/\tau}$ , as shown in the right panel of Fig. 5 (with the angular distribution of  $\rho_{\tau\tau} - \bar{\rho}_{\tau\tau}$  being identical to the  $\rho_{\mu\mu} - \bar{\rho}_{\mu\mu}$  one). The muon and tau lepton number ( $\mu$ LN or  $\tau$ LN) crossings are always much smaller in magnitude than the ELN ones, as shown in Fig. 5, and they tend to become slightly more prominent at larger radii where the flavor instability due to the ELN has already kicked off. As a consequence, in agreement with the findings of Ref. [48] (cf. their Sec. III.C), the growth rate of the flavor instability is driven by the ELN crossing and the  $\mu$ LN and  $\tau$ LN crossings negligibly affect the flavor evolution (results not shown here).

## 6 Heating rate

In order to quantify the impact of flavor evolution computed considering all three flavors vs. the two-flavor approximation, we compute the ratio between the neutrino heating rates

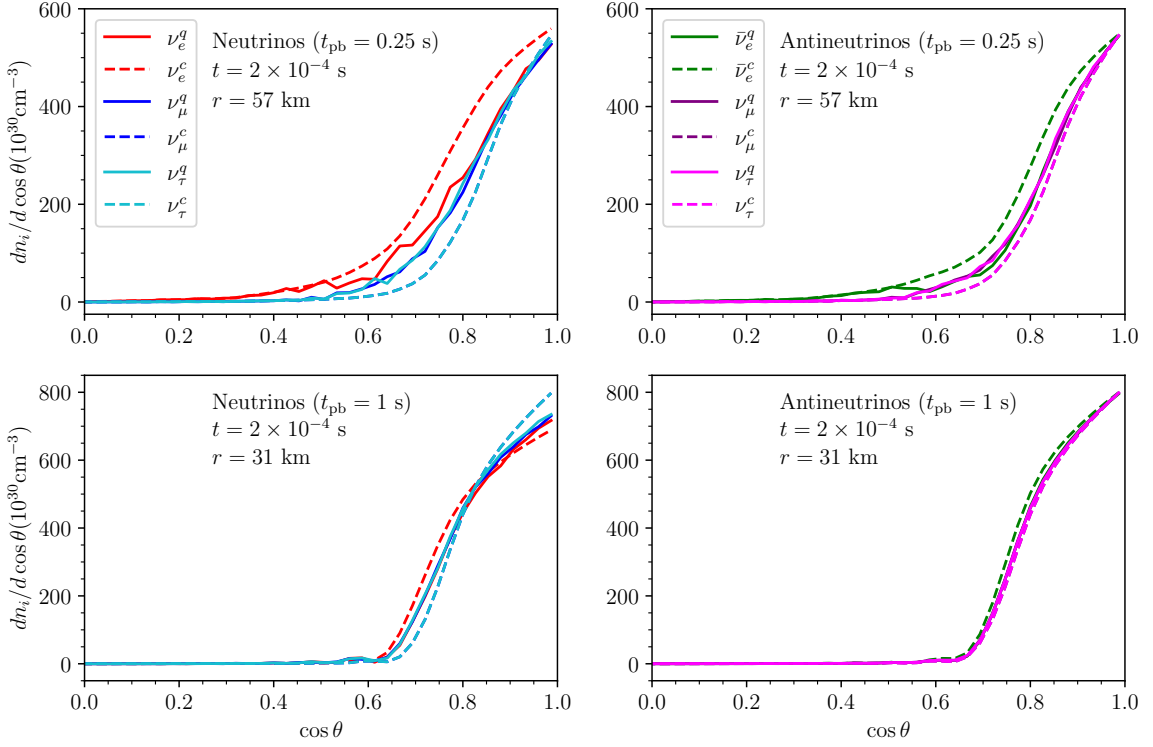


**Figure 4.** Angular distributions for  $\nu_e$  (red),  $\nu_\mu$  (blue), and  $\nu_\tau$  (cyan) on the left panels, and for  $\bar{\nu}_e$  (green),  $\bar{\nu}_\mu$  (violet), and  $\bar{\nu}_\tau$  (magenta) for  $t_{\text{pb}} = 0.25$  s on the top panels and  $t_{\text{pb}} = 1$  s on the bottom. The quasi-steady-state distributions have been extracted at 57 km (31 km) after tracking the flavor evolution for  $2 \times 10^{-4}$  s for  $t_{\text{pb}} = 0.25$  s ( $t_{\text{pb}} = 1$  s); cf. the corresponding energy distributions in Fig. 3. The angular distributions in the absence of flavor conversion are shown as dashed lines, whereas the ones obtained including the flavor evolution are shown as solid lines. Note that the  $x$ -axis ranges between 0 and 1 to improve the plot readability, but the angular distributions extend up to  $\cos \theta = -1$ . The angular distribution of  $\nu_\mu$  is almost identical to that of  $\nu_\tau$  as seen from the left panels and the same is true for  $\bar{\nu}_\mu$  and  $\bar{\nu}_\tau$  as shown in the right panel.

in the (quasi-)steady-state flavor configuration with and without flavor conversion for two and three flavors. The heating rate,  $\dot{\epsilon} = \dot{\epsilon}_{\nu_e} + \dot{\epsilon}_{\bar{\nu}_e}$ , is defined considering

$$\begin{aligned} \dot{\epsilon}_{\nu_e} &= \sigma_0 \left( \frac{1 + 3g_A}{4} \right) \int_0^\infty dE \left( \frac{E + Q}{m_e c^2} \right)^2 \sqrt{(E + Q)^2 - m_e^2} \\ &\quad \times \left[ 1 - \left( \frac{m_e c^2}{E + Q} \right) \right]^{\frac{1}{2}} \left( 1 - 1.01 \frac{E}{m_n} \right) (1 - f_{e^-}) \frac{dn_{\nu_e}}{dE} \end{aligned} \quad (6.1)$$

$$\begin{aligned} \dot{\epsilon}_{\bar{\nu}_e} &= \sigma_0 \left( \frac{1 + 3g_A}{4} \right) \int_{m_e + Q}^\infty dE \left( \frac{E - Q}{m_e c^2} \right)^2 \sqrt{(E - Q)^2 - m_e^2} \\ &\quad \times \left[ 1 - \left( \frac{m_e c^2}{E - Q} \right) \right]^{\frac{1}{2}} \left( 1 - 7.1 \frac{E}{m_p} \right) \frac{dn_{\bar{\nu}_e}}{dE}, \end{aligned} \quad (6.2)$$

where  $Q = 1.2933$  MeV denotes the  $Q$ -value of the beta reaction,  $m_e = 0.511$  MeV is the mass of the electron,  $\sigma_0$  is the characteristic neutrino interaction cross section ( $4G_{\text{F}}^2 m_e^2 / \pi \approx$

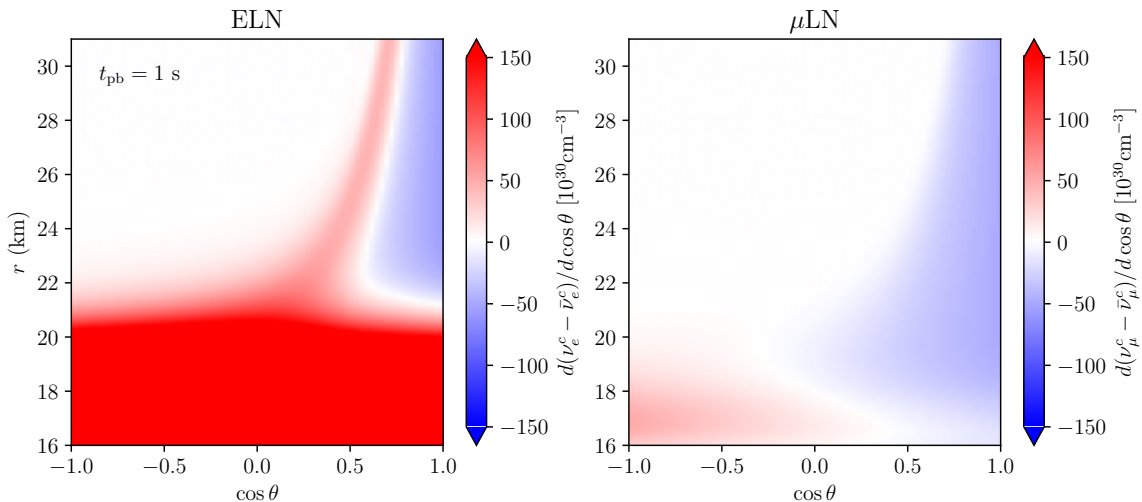


**Figure 5.** *Left:* Heatmap of  $\rho_{ee} - \bar{\rho}_{ee}$  (ELN distribution) in the plane spanned by  $\cos\theta$  and  $r$  in the classical-steady-state configuration for  $t_{\text{pb}} = 1$  s (same as the bottom-left panel of Fig. 1). *Right:* Heatmap of  $\rho_{\mu\mu} - \bar{\rho}_{\mu\mu}$  ( $\mu$ LN distribution) for the same post-bounce time once the weak magnetism corrections are taken into account. The  $\tau$ LN distribution is identical to the  $\mu$ LN one (not shown here). Although  $\mu$ LN and  $\tau$ LN crossings develop due to the weak magnetism corrections, the non-electron crossings negligibly affect flavor conversion.

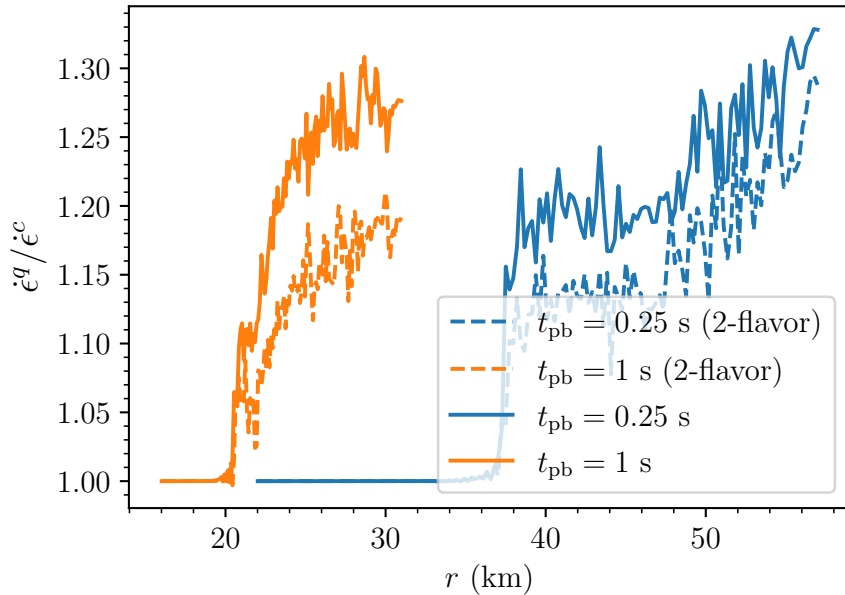
$1.7 \times 10^{-44} \text{ cm}^2$ ) [67],  $(1 - f_{e-})$  is the Pauli-blocking factor of electrons, and  $g_A = 1.27$  is the axial coupling.

Figure 6 shows the radial evolution of the ratio of the heating rates obtained with and without flavor conversion for  $t_{\text{pb}} = 0.25$  s and 1 s. Thanks to flavor evolution, the electron-type neutrinos acquire a high-energy tail; this is a compound effect of the tendency towards flavor equipartition and the fact that the heavy-lepton neutrinos have larger average energies. We find an increase of  $\mathcal{O}(30\%)$  in the heating rate when flavor conversion in three flavors is taken into account. This is due to the fact that neutrino heating is roughly proportional to the third power of neutrino energy.

It is interesting to notice that, in the three-flavor calculation, the quasi-steady-state configuration leads to a higher average energy for electron type neutrinos than in the two-flavor approximation (cf. solid vs. dashed lines in Fig. 6). As a consequence, we find a change in the heating rate triggered by flavor conversion, which is larger by 5–10% in the three-flavor scenario (cf. solid vs. dashed lines in Fig. 6). Moreover, the ratio of the heating rates with and without flavor conversion in two and three flavors is also affected by the fact that the survival probability for  $\bar{\nu}_e$  is approximately 0.3 in three flavors, but is  $\sim 0.5$  in the two-flavor approximation.

## 7 Conclusions

Preliminary work in the context of fast flavor conversion [47, 48] concluded that the solution of the quantum kinetic equations in three flavors for a homogeneous system is different from the one expected in two flavors because of the exponential growth of  $|\rho_{e\mu} - \rho_{e\tau}|$ . In this paper, we investigate the flavor solution of a three-flavor neutrino system which is inhomogeneous and non-stationary. In order to do so, we numerically solve the neutrino quantum kinetic



**Figure 6.** Ratio between the neutrino heating rate obtained in the presence of flavor conversion ( $\dot{\epsilon}^q$ ) and without it ( $\dot{\epsilon}^c$ ) when the (quasi-)steady-state flavor configuration is achieved. The solid lines represent the heating rates computed in the three flavor framework, while the dashed lines have been computed in the two-flavor approximation for  $t_{\text{pb}} = 0.25$  s (blue) and  $t_{\text{pb}} = 1$  s (orange). Thanks to neutrino flavor evolution, the electron-type neutrinos acquire a high energy tail due to which the heating rate increases by approximately 30%. With respect to the two-flavor solution, the heating rate increases by about 5% for  $t_{\text{pb}} = 0.25$  s and by 10% for  $t_{\text{pb}} = 1$  s.

equations in a multi-energy and multi-angle framework, relying on static hydrodynamic and thermodynamic inputs from a  $18.6M_{\odot}$  spherically symmetric core-collapse supernova simulation. Because of the challenges intrinsic to the solution of the quantum kinetic equations, we focus on a spherically symmetric shell in the surroundings of neutrino decoupling. We show our findings for two representative post-bounce times,  $t_{\text{pb}} = 0.25$  and 1 s, as examples of cases where the flavor conversion is triggered by slow collective oscillations in the absence of ELN crossings (in the first case) and where flavor conversion is triggered by fast instabilities (for  $t_{\text{pb}} = 1$  s). First, we neglect flavor conversion and compute the angular distributions of neutrinos and antineutrinos. Then, we adopt such classical-steady-state flavor configuration to solve the quantum kinetic equations in the presence of flavor conversion, until a quasi-steady-state configuration is reached after  $10^{-4}$  s.

We find that, for both post-bounce times, flavor equipartition is achieved in the antineutrino sector, in the sense that the  $\bar{\nu}_e$  energy spectrum becomes comparable to the one of  $\bar{\nu}_x = (\bar{\nu}_{\mu} + \bar{\nu}_{\tau})/2$ . For neutrinos, equipartition is achieved for  $t_{\text{pb}} = 1$  s, but not for  $t_{\text{pb}} = 0.25$  s. This difference is due to the fact that, at late post-bounce times, the neutrino emission properties across different flavors tend to approach each other, while a larger difference among the neutrino emission properties of all flavors exists at earlier post-bounce times. In agreement with Refs. [47, 48], the exponential growth of  $|\rho_{e\mu} - \rho_{e\tau}|$  is responsible for differences between the quasi-steady-state three-flavor configuration and the one obtained adopting the two-flavor approximation. In particular, flavor equipartition implies a survival

probability of  $\sim 1/3$  for antineutrinos in three flavors as opposed to a survival probability of  $\sim 1/2$  in the two flavors. We find that these conclusions hold for all flavor configurations with an ELN crossing, corresponding to post-bounce times  $t_{\text{pb}} \gtrsim 0.5$  s for our benchmark supernova model.

The weak magnetism corrections to the interaction rates are responsible for the creation of crossings in the angular distributions of the muon and tau neutrino lepton numbers (while they negligibly affect the ELN distributions because beta processes dominate the interaction rate). Such muon/tau crossings have a smaller magnitude than the ELN ones and give rise to fast instabilities with a smaller growth rate. As a consequence, we find that muon/tau crossings negligibly affect the flavor evolution history.

In conclusion, our findings suggest that one should expect a larger impact of flavor conversion on the heating rate when all three neutrino flavors are taken into account. We find a  $\mathcal{O}(30\%)$  increase in the heating rate in three flavors, which is larger by 5–10% with respect to the analog two-flavor solution.

## Acknowledgments

This project has received support from the Villum Foundation (Project No. 13164), the Danmarks Frie Forskningsfond (Project No. 8049-00038B), the European Union (ERC, ANET, Project No. 101087058), and the Deutsche Forschungsgemeinschaft through Sonderforschungsbereich SFB 1258 “Neutrinos and Dark Matter in Astro- and Particle Physics” (NDM). Views and opinions expressed are those of the authors only and do not necessarily reflect those of the European Union or the European Research Council. Neither the European Union nor the granting authority can be held responsible for them. The Tycho supercomputer hosted at the SCIENCE HPC Center at the University of Copenhagen was used for supporting the numerical simulations presented in this work.

## A Matter background and neutrino self-interaction

In the neutrino equations of motion, neutrino refraction on the matter background formally leads to a precession with respect to the interaction direction, similar to the vacuum mixing term. Therefore, within the neutrino bulb-model, refraction of neutrinos off electrons has been neglected, in lieu of a small effective vacuum mixing angle [68]. Such effective mixing angle (expected to be smaller as the matter density increases) shifts the onset radius of collective flavor conversion to larger radii [43, 68–70]. As the matter density increases, one can reach the extreme situation of flavor conversion never being triggered. In fact, early work in this direction concluded that neutrino-neutrino flavor transformation can be suppressed in the core of a core-collapse supernova, during the accretion phase when the electron matter density is significantly larger than the neutrino one [71, 72]. However, the neutrino angular distributions are not semi-isotropic in the decoupling region, they are forward peaked. In addition, within the neutrino-bulb model, the time dependence is ignored in the equations of motion, assuming that the flavor content is in steady state at any time; recent understanding of neutrino flavor conversion as a dynamical phenomenon happening in an inhomogeneous medium highlights the importance of both time and spatial dependence in the solution of the quantum kinetic equations of neutrinos [32, 33, 38, 39, 65, 66, 73–76].

In light of these recent developments, in this appendix, we reexamine the role of dense matter background to understand whether the matter suppression of flavor transformation

still holds in a non-stationary neutrino ensemble and for anisotropic neutrino angular distributions. First, we consider the case of the neutrino bulb model and then explore the role of matter in the solution of time- and space-dependent quantum kinetic equations

### A.1 Neutrino bulb model

In the neutrino-bulb model [25], Eqs. 2.1 and 2.2 simplify through the following assumptions.

- Neutrino decoupling from matter is modeled assuming that neutrinos are emitted from a sphere of radius  $R_\nu$  (the neutrinosphere), identical for all flavors. (and not from extended flavor-dependent regions as assumed in this work).
- The collision terms in Eqs. 2.1 and 2.2 are neglected ( $\mathcal{C} = \bar{\mathcal{C}} = 0$ ), and neutrinos are emitted semi-isotropically in the outward direction and uniformly from the neutrinosphere.
- (Anti)neutrinos are emitted in pure flavor eigenstates from the neutrinosphere.
- The (anti)neutrino ensemble is assumed to be in a steady state (i.e., the time scale of neutrino self-interaction is fast compared to the time scale over which the neutrino density changes).

For a given neutrino trajectory, the angle  $\theta$  is a function of  $r$  and the emission angle ( $\theta_0$ ) in the bulb model [25]:

$$\cos \theta = \sqrt{1 - \left(\frac{R_\nu}{r}\right)^2 (1 - \cos^2 \theta_0)} . \quad (\text{A.1})$$

Since the (anti)neutrino ensemble is stationary, time and radius are related for a particular trajectory. At a given location, the time required for the neutrinos to reach a given location depends on the angle relative to the radial direction:

$$ct = r \cos \theta - R_\nu \cos \theta_0 , \quad (\text{A.2})$$

$$cdt = dr \cos \theta , \quad (\text{A.3})$$

where we see that the time required to reach a given location is larger for a trajectory with a larger angle  $\theta$  with respect to the radial direction. Hence Eqs. 2.1 and 2.2 become dependent on radius (and not time) in the neutrino bulb-model.

The temporal evolution of the density matrix describing the neutrino field along a certain trajectory is given by

$$\rho(t) = \exp_T \left( -i \int_0^t H(E', \cos \theta', r', t') dt' \right) \rho(0) \exp_T \left( i \int_0^t H(E', \cos \theta', r', t') dt' \right) , \quad (\text{A.4})$$

where the subscript  $T$  of the exponential denotes the time ordering. The corresponding radial distance traveled by neutrinos within the time  $t$  depends on the angle  $\theta$ , as illustrated in Eq. A.2. If we intend to investigate the radial evolution of neutrino flavor, it is more convenient to use the following expression:

$$\rho(r) = \exp_T \left( -i \int_{R_\nu}^r H(E', \cos \theta', r') \frac{dr'}{c \cos \theta'} \right) \rho(R_\nu) \exp_T \left( i \int_{R_\nu}^r H(E', \cos \theta', r') \frac{dr'}{c \cos \theta'} \right) , \quad (\text{A.5})$$

where we use Eq. A.3 to account for the longer path length associated with neutrinos with a larger emission angle. It is important to note that the Hamiltonian is rescaled by a factor  $1/(c \cos \theta)$  to consider that neutrinos with a larger emission angle travel a longer distance. This led to conclude that matter suppresses flavor conversion in the accretion phase of a core-collapse supernova [72].

## A.2 Matter effects on flavor transformation in the quantum kinetic approach

We now investigate the role of matter in flavor conversion relaxing the simplifying assumptions characterizing the bulb model and relying on Eqs. 2.1 and 2.2. This means that we now do not consider a stationary neutrino ensemble. In this case, the motion of neutrinos is taken into account through the additive term (vs. in the time-independent formalism, a multiplicative factor  $1/\cos \theta$  appears). Hence, we should expect a qualitatively different impact of matter on the flavor evolution, since the background matter should suppress flavor instabilities in space but not in time [77, 78], and a partial cancellation of matter effects occurs for a non-stationary neutrino gas [79, 80].

Equations 2.1 and 2.2 include the advective term ( $\vec{v} \cdot \nabla$ ) which is responsible for hindering matter suppression of flavor conversion. In fact, if we assume that the advective term suppresses the flavor instability in the presence of a significant matter term, then the term  $\vec{v} \cdot \nabla \rho_{ex}$  should be small at the radius where the system transitions from flavor stable to flavor unstable ( $r_{\text{instab}}$ ). This implies that the system should behave like a homogeneous gas at  $r_{\text{instab}}$  and hence be unstable [24, 71]. Matter cannot suppress the neutrino flavor instability due to the advective term. This fact can be demonstrated by performing numerical simulations in the time-dependent formalism with and without the matter term, as shown in the following.

We focus on the post-bounce time  $t_{\text{pb}} = 0.05$  s, which exhibits flavor instability due to the vacuum term (without ELN crossings). We deliberately choose this configuration because, in the presence of ELN crossings, the growth rate of fast conversion is very large, and matter suppression is not feasible. In order to make the problem tractable, we use a suppression factor  $\xi = 10^{-3}$  in Eq. 2.7; note that this is different than the case considered in the main text where  $\xi = 10^{-2}$  in order to minimize the computational time, however, our conclusions should not qualitatively depend on the choice of  $\xi$ .

We investigate the flavor evolution in three different settings as summarized in Table 1

- Case A. We assume  $\lambda = 0$  in Eqs. 2.1 and 2.2 and small effective mixing angles:  $\theta_{12} = \theta_{23} = \theta_{13} = 10^{-3}$  rad. This is the setup adopted in the main text.
- Case B. We adopt the best-fit values from Ref. [61] for the mass and mixing parameters, although we assume  $\delta_{\text{CP}} = 0$  for the sake of simplicity. We adopt inputs from the supernova simulation to compute the matter potential  $\lambda$ , but we suppress it by a constant factor  $10^{-2}$  and adopt  $\lambda = 10^3 \text{ km}^{-1}$  in the innermost radial region where  $\lambda$  would be too large preventing an efficient numerical solution.
- Case C. This case is identical to Case B, except for the fact that the matter potential is suppressed by a factor  $10^{-3}$  instead of  $10^{-2}$ .

We note that, although the matter Hamiltonian is not as large as it would be in the supernova core, it is still very large compared to the vacuum frequency. Also, unlike the case of the neutrino-bulb model, we have non-trivial angular distributions, which lead to the development



**Table 1.** Summary of the three different scenarios adopted to investigate whether matter suppresses flavor conversion in a time-dependent, inhomogeneous neutrino gas. The neutrino mass-mixing parameters are the best-fit values reported in Ref. [61].

	Case A	Case B	Case C
$\delta m^2$ (eV <sup>2</sup> )	$7.5 \times 10^{-5}$	$7.5 \times 10^{-5}$	$7.5 \times 10^{-5}$
$\Delta m^2$ (eV <sup>2</sup> )	$2.5 \times 10^{-3}$	$2.5 \times 10^{-3}$	$2.5 \times 10^{-3}$
$\vartheta_V^{12}$ (rad)	$10^{-3}$	0.59	0.59
$\vartheta_V^{23}$ (rad)	$10^{-3}$	0.86	0.86
$\vartheta_V^{13}$ (rad)	$10^{-3}$	0.15	0.15
$\delta_{\mathcal{CP}}$	0	0	0
$\lambda$ (km <sup>-1</sup> )	0	$\min(10^3, 10^{-2}\sqrt{2}G_{\text{F}}n_e)$	$\min(10^3, 10^{-3}\sqrt{2}G_{\text{F}}n_e)$

of flavor instabilities at a much larger density. Hence, the matter suppression would have been much more pronounced if present.

Figures 7 and 8 show the results of flavor evolution in the three different Cases at  $t = 5 \times 10^{-4}$  s. We can see that, irrespective of whether effective mixing angles or  $\lambda$  are adopted, the final flavor configuration is almost identical in all three Cases. This highlights that matter suppression does not occur in the presence of large  $\lambda$ , contrary to what is expected in the bulb model. Moreover, Fig. 7 and 8 also justify the employment of effective mixing angles in numerical simulations of time-dependent, inhomogeneous neutrino gases, instead of the realistic matter potential that would make the numerical solution of the quantum kinetic equations much more expensive. We stress that the suppression of the mixing angle due to the matter effects is justified, if we assume that neutrinos are emitted in flavor eigenstates. In the next appendix, we argue that the emission of neutrinos in a supernova is not in flavor eigenstates strictly speaking.

## B Are neutrinos emitted as flavor eigenstates in the interior of a core-collapse supernova?

It is generally assumed that neutrinos are emitted in flavor eigenstates in the interior of a core-collapse supernova. In this appendix, we show that the density matrix of neutrinos emitted in the interior of a core-collapse supernova is not diagonal in the flavor basis, but has small off-diagonal components. This is due to the fact that, in the supernova core, (anti)neutrinos undergo neutral-current interactions (i.e., pair-production and Bremsstrahlung).

The beta process is a charged-current one, leading to the emission of neutrinos in a particular flavor eigenstate. However, pair production and Bremsstrahlung processes are neutral-current reactions and therefore neutrinos are not emitted as flavor eigenstates. In fact, the wave function of neutrinos emitted in a  $Z$ -boson decay is a linear superposition of entangled states of a neutrino with an antineutrino, with all flavor states being equally likely. If the flavor of the neutrino or antineutrino is measured, the wave function of the other particle collapses to a flavor eigenstate. However, in the context of the mean-field approach, one can ignore the entanglement and trace over the antineutrinos to find the wave function of neutrinos and vice-versa. The single particle wave functions can thus be described as  $\psi_\nu \sim |\nu_e\rangle + |\nu_\mu\rangle + |\nu_\tau\rangle$  and  $\psi_{\bar{\nu}} \sim |\bar{\nu}_e\rangle + |\bar{\nu}_\mu\rangle + |\bar{\nu}_\tau\rangle$ . This form of the wave function implies that the emitted neutrino can be thought of as a linear superposition of three flavor eigenstates. Hence, the density matrix is not diagonal in the flavor basis. Similar

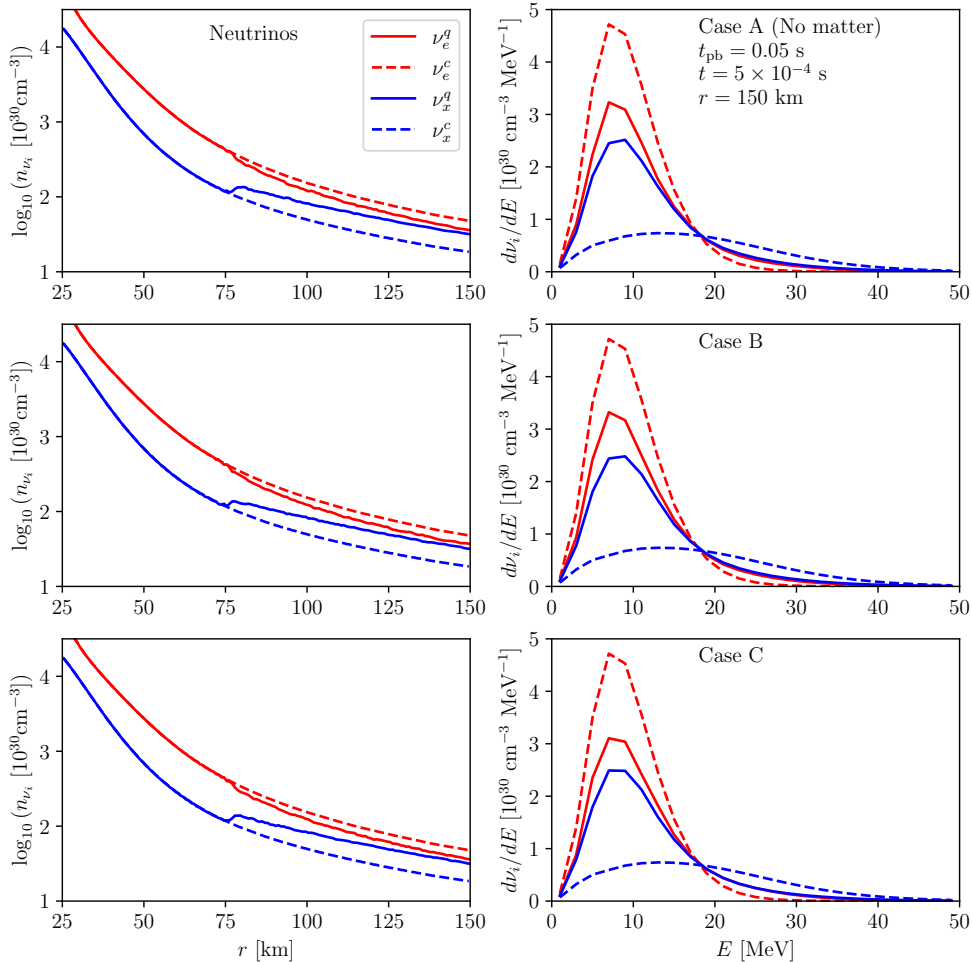


**Figure 7.** *Left:* Radial dependence of the neutrino number density for Cases A, B, and C, from top to bottom respectively (cf. Table 1). The red solid (dashed) line shows the number density for  $\nu_e$  with (without) flavor evolution at  $t = 5 \times 10^{-4} \text{ s}$ . The blue solid (dashed) line shows the number density for  $\nu_x$  with (without) flavor evolution. The number density of  $\nu_x$  is defined as the average between the  $\nu_\mu$  and  $\nu_\tau$  number densities. *Right:* Energy spectra of  $\nu_e$  and  $\nu_x$  extracted at  $r = 150 \text{ km}$ . The neutrino densities, after flavor conversion, are comparable among Cases A, B, and C.

conclusions hold for the pair production process, but neutrinos cannot be maximally mixed as they undergo charge-current and neutral-current interactions. Since it is more likely for electron-type neutrinos to be emitted in the pair production processes, the emission term corresponding to the off-diagonal correction of the density matrix should be given by the geometric mean of the diagonal emission terms.

The emission term for electron type neutrinos is dominated by the beta processes, therefore the off-diagonal term is much smaller than the diagonal one. In the absence of

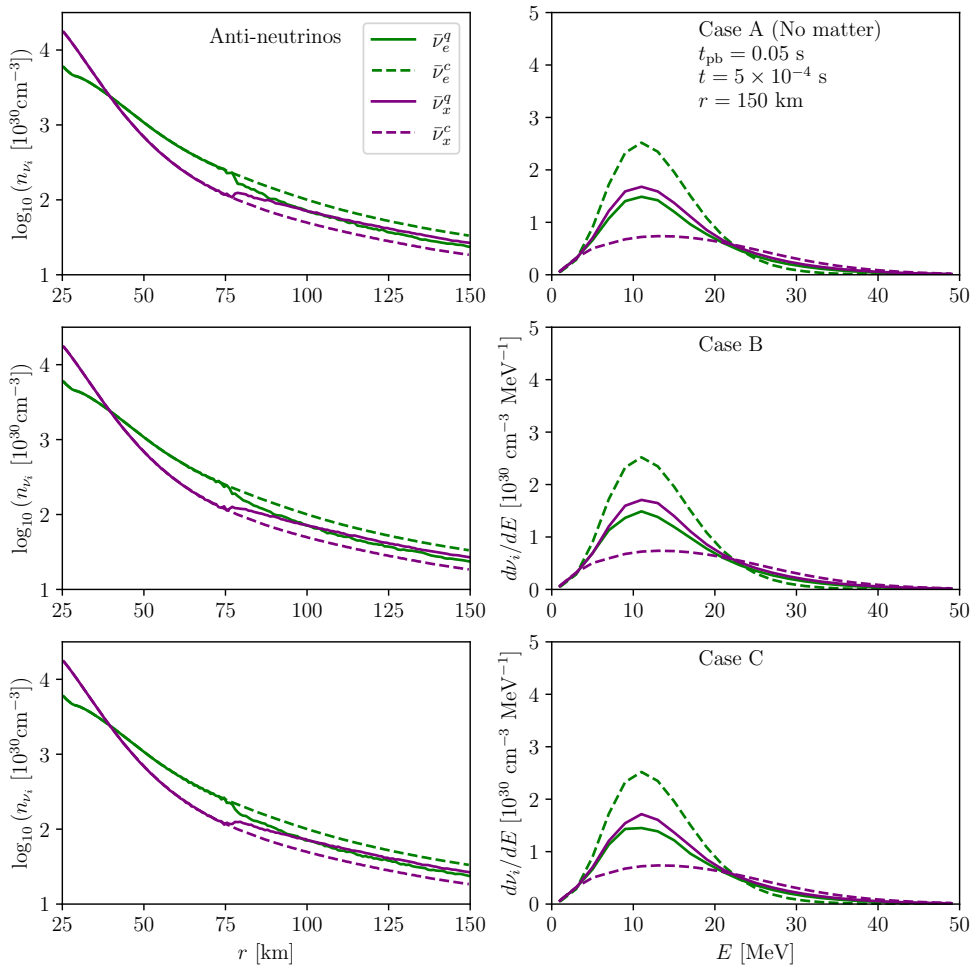


**Figure 8.** Same as Fig. 7 but for antineutrinos. The  $\bar{\nu}_e$  ( $\bar{\nu}_x = \bar{\nu}_\mu + \bar{\nu}_\tau$ ) number density is plotted in green (purple).

emission, the vacuum suppressed mixing angle is the only source of the initial perturbation to the off-diagonal component of the Hamiltonian. However, the off-diagonal component of the emission term can dominate over the off-diagonal seed due to vacuum mixing because of the large matter density. The perturbation provided by the off-diagonal component of the emission term can be considered as an effective mixing angle:

$$\tan(2\theta_{\text{eff}}) \approx \frac{\mathcal{C}_{ex}^{\text{emit}}}{\mathcal{C}_e^{\text{emit}} - \mathcal{C}_x^{\text{emit}}} . \quad (\text{B.1})$$

Calculating the geometric mean of the diagonal components for each process for our benchmark model, we find that the effective value of this mixing angle is  $\mathcal{O}(10^{-3})$ . This effective mixing angle is energy dependent. However, as shown in Appendix A, the quasi-steady-state

flavor configuration is not sensitive to the specific value of the effective mixing angles as long as they are not very small.

We have solved the quantum kinetic equations assuming non-zero off-diagonal terms in the emission term of the collisional rate (leading to non-zero off-diagonal seeds in the density matrices in the absence of oscillations) in our initial flavor configuration. The term  $C_{ex}^{\text{emit}}$  also provides a small initial perturbation for the off-diagonal component of the Hamiltonian. We find that the quasi-steady-state flavor configuration depends negligibly on the inclusion of such correction (results not shown here).

## References

- [1] L. Wolfenstein, *Neutrino oscillations in matter*, *Phys. Rev. D* **17** (May, 1978) 2369–2374.
- [2] S. P. Mikheyev and A. Yu. Smirnov, *Resonance enhancement of oscillations in matter and solar neutrino spectroscopy*, *Yadernaya Fizika* **42** (1985) 1441–1448.
- [3] S. P. Mikheev and A. Yu. Smirnov, *Neutrino Oscillations in a Variable Density Medium and Neutrino Bursts Due to the Gravitational Collapse of Stars*, *Sov. Phys. JETP* **64** (1986) 4–7, [[0706.0454](#)].
- [4] J. T. Pantaleone, *Neutrino oscillations at high densities*, *Phys. Lett. B* **287** (1992) 128–132.
- [5] I. Tamborra and S. Shalgar, *New Developments in Flavor Evolution of a Dense Neutrino Gas*, *Ann. Rev. Nucl. Part. Sci.* **71** (2021) 165–188, [[2011.01948](#)].
- [6] S. Richers and M. Sen, *Fast Flavor Transformations*, pp. 1–17. Springer Nature Singapore, Singapore, 2022. [[2207.03561](#)]. 10.1007/978-981-15-8818-1-125-1.
- [7] M. C. Volpe, *Neutrinos from dense environments: Flavor mechanisms, theoretical approaches, observations, and new directions*, *Rev. Mod. Phys.* **96** (2024) 025004, [[2301.11814](#)].
- [8] I. Tamborra, *Neutrinos from explosive transients at the dawn of multi-messenger astronomy*, [2412.09699](#).
- [9] J. Ehring, S. Abbar, H.-T. Janka, G. G. Raffelt and I. Tamborra, *Fast Neutrino Flavor Conversions Can Help and Hinder Neutrino-Driven Explosions*, *Phys. Rev. Lett.* **131** (2023) 061401, [[2305.11207](#)].
- [10] J. Ehring, S. Abbar, H.-T. Janka, G. G. Raffelt and I. Tamborra, *Fast neutrino flavor conversion in core-collapse supernovae: A parametric study in 1D models*, *Phys. Rev. D* **107** (2023) 103034, [[2301.11938](#)].
- [11] K. Mori, T. Takiwaki, K. Kotake and S. Horiuchi, *Three-dimensional core-collapse supernova models with phenomenological treatment of neutrino flavor conversions*, [2501.15256](#).
- [12] M. George, M.-R. Wu, I. Tamborra, R. Ardevol-Pulpillo and H.-T. Janka, *Fast neutrino flavor conversion, ejecta properties, and nucleosynthesis in newly-formed hypermassive remnants of neutron-star mergers*, *Phys. Rev. D* **102** (2020) 103015, [[2009.04046](#)].
- [13] M.-R. Wu and I. Tamborra, *Fast neutrino conversions: Ubiquitous in compact binary merger remnants*, *Phys. Rev. D* **95** (2017) 103007, [[1701.06580](#)].
- [14] M.-R. Wu, I. Tamborra, O. Just and H.-T. Janka, *Imprints of neutrino-pair flavor conversions on nucleosynthesis in ejecta from neutron-star merger remnants*, *Phys. Rev. D* **96** (2017) 123015, [[1711.00477](#)].
- [15] X. Li and D. M. Siegel, *Neutrino Fast Flavor Conversions in Neutron-Star Postmerger Accretion Disks*, *Phys. Rev. Lett.* **126** (2021) 251101, [[2103.02616](#)].
- [16] R. Fernández, S. Richers, N. Mulyk and S. Fahlman, *Fast flavor instability in hypermassive neutron star disk outflows*, *Phys. Rev. D* **106** (2022) 103003, [[2207.10680](#)].

- [17] R. F. Sawyer, *Speed-up of neutrino transformations in a supernova environment*, *Phys. Rev. D* **72** (2005) 045003, [[hep-ph/0503013](#)].
- [18] R. F. Sawyer, *The multi-angle instability in dense neutrino systems*, *Phys. Rev. D* **79** (2009) 105003, [[0803.4319](#)].
- [19] R. F. Sawyer, *Neutrino cloud instabilities just above the neutrino sphere of a supernova*, *Phys. Rev. Lett.* **116** (2016) 081101, [[1509.03323](#)].
- [20] S. Chakraborty, R. S. Hansen, I. Izaguirre and G. G. Raffelt, *Self-induced neutrino flavor conversion without flavor mixing*, *JCAP* **03** (2016) 042, [[1602.00698](#)].
- [21] I. Izaguirre, G. G. Raffelt and I. Tamborra, *Fast Pairwise Conversion of Supernova Neutrinos: A Dispersion-Relation Approach*, *Phys. Rev. Lett.* **118** (2017) 021101, [[1610.01612](#)].
- [22] T. Morinaga, *Fast neutrino flavor instability and neutrino flavor lepton number crossings*, *Phys. Rev. D* **105** (2022) L101301, [[2103.15267](#)].
- [23] D. F. G. Fiorillo and G. G. Raffelt, *Theory of neutrino fast flavor evolution. Part I. Linear response theory and stability conditions.*, *JHEP* **08** (2024) 225, [[2406.06708](#)].
- [24] H. Duan, G. M. Fuller and Y.-Z. Qian, *Collective neutrino flavor transformation in supernovae*, *Phys. Rev. D* **74** (2006) 123004, [[astro-ph/0511275](#)].
- [25] H. Duan, G. M. Fuller, J. Carlson and Y.-Z. Qian, *Simulation of Coherent Non-Linear Neutrino Flavor Transformation in the Supernova Environment. 1. Correlated Neutrino Trajectories*, *Phys. Rev. D* **74** (2006) 105014, [[astro-ph/0606616](#)].
- [26] H. Duan, G. M. Fuller, J. A. Carlson and Y.-Z. Qian, *Coherent Development of Neutrino Flavor in the Supernova Environment*, *Phys. Rev. Lett.* **97** (2006) 241101, [[astro-ph/0608050](#)].
- [27] G. Fogli, E. Lisi, A. Marrone and A. Mirizzi, *Collective neutrino flavor transitions in supernovae and the role of trajectory averaging*, *JCAP* **0712** (2007) 010, [[0707.1998](#)].
- [28] H. Duan, G. M. Fuller and Y.-Z. Qian, *Collective Neutrino Oscillations*, *Ann. Rev. Nucl. Part. Sci.* **60** (2010) 569–594, [[1001.2799](#)].
- [29] D. F. G. Fiorillo and G. G. Raffelt, *Slow and fast collective neutrino oscillations: Invariants and reciprocity*, *Phys. Rev. D* **107** (2023) 043024, [[2301.09650](#)].
- [30] D. F. G. Fiorillo and G. G. Raffelt, *Theory of neutrino slow flavor evolution. Part II. Space-time evolution of linear instabilities*, [2501.16423](#).
- [31] P. Dedin Neto, I. Tamborra and S. Shalgar, *Fast Conversion of Neutrinos: Energy Dependence of Flavor Instabilities*, [2312.06556](#).
- [32] S. Shalgar and I. Tamborra, *Neutrino quantum kinetics in a core-collapse supernova*, *JCAP* **09** (2024) 021, [[2406.09504](#)].
- [33] I. Padilla-Gay, S. Shalgar and I. Tamborra, *Multi-Dimensional Solution of Fast Neutrino Conversions in Binary Neutron Star Merger Remnants*, *JCAP* **01** (2021) 017, [[2009.01843](#)].
- [34] S. Shalgar and I. Tamborra, *A change of direction in pairwise neutrino conversion physics: The effect of collisions*, *Phys. Rev. D* **103** (2021) 063002, [[2011.00004](#)].
- [35] H. Nagakura and M. Zaizen, *Time-Dependent and Quasisteady Features of Fast Neutrino-Flavor Conversion*, *Phys. Rev. Lett.* **129** (2022) 261101, [[2206.04097](#)].
- [36] C. Kato, H. Nagakura and M. Zaizen, *Flavor conversions with energy-dependent neutrino emission and absorption*, *Phys. Rev. D* **108** (2023) 023006, [[2303.16453](#)].
- [37] H. Nagakura and M. Zaizen, *Basic characteristics of neutrino flavor conversions in the postshock regions of core-collapse supernova*, *Phys. Rev. D* **108** (2023) 123003, [[2308.14800](#)].

- [38] Z. Xiong, M.-R. Wu, M. George, C.-Y. Lin, N. K. Largani, T. Fischer et al., *Fast neutrino flavor conversions in a supernova: Emergence, evolution, and effects*, *Phys. Rev. D* **109** (2024) 123008, [2402.19252].
- [39] Z. Xiong, M.-R. Wu, M. George and C.-Y. Lin, *Robust Integration of Fast Flavor Conversions in Classical Neutrino Transport*, *Phys. Rev. Lett.* **134** (2025) 051003, [2403.17269].
- [40] J. Liu, H. Nagakura, M. Zaizen, L. Johns, R. Akaho and S. Yamada, *Quasisteady evolution of fast neutrino-flavor conversions*, *Phys. Rev. D* **111** (2025) 023051, [2411.08503].
- [41] G. Fogli, E. Lisi, A. Marrone and I. Tamborra, *Supernova neutrino three-flavor evolution with dominant collective effects*, *JCAP* **04** (2009) 030, [0812.3031].
- [42] B. Dasgupta, A. Mirizzi, I. Tamborra and R. Tomas, *Neutrino mass hierarchy and three-flavor spectral splits of supernova neutrinos*, *Phys. Rev. D* **81** (2010) 093008, [1002.2943].
- [43] B. Dasgupta, G. G. Raffelt and I. Tamborra, *Triggering collective oscillations by three-flavor effects*, *Phys. Rev. D* **81** (2010) 073004, [1001.5396].
- [44] B. Dasgupta and A. Dighe, *Collective three-flavor oscillations of supernova neutrinos*, *Phys. Rev. D* **77** (2008) 113002, [0712.3798].
- [45] B. Dasgupta, A. Dighe, A. Mirizzi and G. G. Raffelt, *Spectral split in prompt supernova neutrino burst: Analytic three-flavor treatment*, *Phys. Rev. D* **77** (2008) 113007, [0801.1660].
- [46] A. Friedland, *Self-refraction of supernova neutrinos: mixed spectra and three-flavor instabilities*, *Phys. Rev. Lett.* **104** (2010) 191102, [1001.0996].
- [47] M. Chakraborty and S. Chakraborty, *Three flavor neutrino conversions in supernovae: slow & fast instabilities*, *JCAP* **01** (2020) 005, [1909.10420].
- [48] S. Shalgar and I. Tamborra, *Three flavor revolution in fast pairwise neutrino conversion*, *Phys. Rev. D* **104** (2021) 023011, [2103.12743].
- [49] R. Bollig, H.-T. Janka, A. Lohs, G. Martinez-Pinedo, C. J. Horowitz and T. Melson, *Muon Creation in Supernova Matter Facilitates Neutrino-driven Explosions*, *Phys. Rev. Lett.* **119** (2017) 242702, [1706.04630].
- [50] E. Loffredo, A. Perego, D. Logoteta and M. Branchesi, *Muons in the aftermath of neutron star mergers and their impact on trapped neutrinos*, *Astron. Astrophys.* **672** (2023) A124, [2209.04458].
- [51] H. H.-Y. Ng, C. Musolino, S. D. Tootle and L. Rezzolla, *Accurate muonic interactions in neutron-star mergers and impact on heavy-element nucleosynthesis*, 2411.19178.
- [52] M. A. Pajkos and E. R. Most, *Influence of muons, pions, and trapped neutrinos on neutron star mergers*, *Phys. Rev. D* **111** (2025) 043013, [2409.09147].
- [53] F. Capozzi, S. Abbar, R. Bollig and H.-T. Janka, *Fast neutrino flavor conversions in one-dimensional core-collapse supernova models with and without muon creation*, *Phys. Rev. D* **103** (2021) 063013, [2012.08525].
- [54] S. Airen, F. Capozzi, S. Chakraborty, B. Dasgupta, G. G. Raffelt and T. Stirner, *Normal-mode Analysis for Collective Neutrino Oscillations*, *JCAP* **12** (2018) 019, [1809.09137].
- [55] F. Capozzi, M. Chakraborty, S. Chakraborty and M. Sen, *Fast flavor conversions in supernovae: the rise of mu-tau neutrinos*, *Phys. Rev. Lett.* **125** (2020) 251801, [2005.14204].
- [56] E. Grohs, S. Richers, S. M. Couch, F. Foucart, J. P. Kneller and G. C. McLaughlin, *Neutrino fast flavor instability in three dimensions for a neutron star merger*, *Phys. Lett. B* **846** (2023) 138210, [2207.02214].
- [57] H. R. Purcell, S. Richers, A. V. Patwardhan and F. Foucart, *Three-flavor, full momentum space neutrino spin oscillations in neutron star mergers*, *Phys. Rev. D* **110** (2024) 023003, [2404.08159].



- [58] “Garching core-collapse supernova data archive.”  
<https://wwwmpa.mpa-garching.mpg.de/ccsnarchive/data/Bollig2016/>.
- [59] G. Sigl and G. G. Raffelt, *General kinetic description of relativistic mixed neutrinos*, *Nucl. Phys. B* **406** (1993) 423–451.
- [60] M. A. Rudzkii, *Kinetic equations for neutrino spin- and type-oscillations in a medium*, *Astrophys. and Space Science* **165** (Mar., 1990) 65–81.
- [61] “Nufit.” <http://www.nu-fit.org/>.
- [62] S. Shalgar and I. Tamborra, *Do neutrinos become flavor unstable due to collisions with matter in the supernova decoupling region?*, *Phys. Rev. D* **109** (2024) 103011, [2307.10366].
- [63] H.-T. Janka, K. Langanke, A. Marek, G. Martinez-Pinedo and B. Mueller, *Theory of Core-Collapse Supernovae*, *Phys. Rept.* **442** (2007) 38–74, [astro-ph/0612072].
- [64] I. Tamborra, L. Huedepohl, G. G. Raffelt and H.-T. Janka, *Flavor-dependent neutrino angular distribution in core-collapse supernovae*, *Astrophys. J.* **839** (2017) 132, [1702.00060].
- [65] S. Shalgar and I. Tamborra, *Neutrino decoupling is altered by flavor conversion*, *Phys. Rev. D* **108** (2023) 043006, [2206.00676].
- [66] S. Shalgar and I. Tamborra, *Neutrino flavor conversion, advection, and collisions: Toward the full solution*, *Phys. Rev. D* **107** (2023) 063025, [2207.04058].
- [67] T. A. Thompson, *Topics in the theory of core-collapse supernovae*, Ph.D. thesis, The University of Arizona., 2002.
- [68] S. Hannestad, G. G. Raffelt, G. Sigl and Y. Y. Y. Wong, *Self-induced conversion in dense neutrino gases: Pendulum in flavour space*, *Phys. Rev. D* **74** (2006) 105010, [astro-ph/0608695].
- [69] H. Duan, G. M. Fuller, J. Carlson and Y.-Z. Qian, *Analysis of Collective Neutrino Flavor Transformation in Supernovae*, *Phys. Rev. D* **75** (2007) 125005, [astro-ph/0703776].
- [70] B. Dasgupta, E. P. O’Connor and C. D. Ott, *The Role of Collective Neutrino Flavor Oscillations in Core-Collapse Supernova Shock Revival*, *Phys. Rev. D* **85** (2012) 065008, [1106.1167].
- [71] A. Esteban-Pretel, A. Mirizzi, S. Pastor, R. Tomàs, G. G. Raffelt, P. D. Serpico et al., *Role of dense matter in collective supernova neutrino transformations*, *Phys. Rev. D* **78** (2008) 085012, [0807.0659].
- [72] S. Chakraborty, T. Fischer, A. Mirizzi, N. Saviano and R. Tomas, *Analysis of matter suppression in collective neutrino oscillations during the supernova accretion phase*, *Phys. Rev. D* **84** (2011) 025002, [1105.1130].
- [73] S. Shalgar, I. Padilla-Gay and I. Tamborra, *Neutrino propagation hinders fast pairwise flavor conversions*, *JCAP* **06** (2020) 048, [1911.09110].
- [74] H. Nagakura, *General-relativistic quantum-kinetics neutrino transport*, *Phys. Rev. D* **106** (2022) 063011, [2206.04098].
- [75] H. Nagakura and M. Zaizen, *Connecting small-scale to large-scale structures of fast neutrino-flavor conversion*, *Phys. Rev. D* **107** (2023) 063033, [2211.01398].
- [76] M. Cornelius, S. Shalgar and I. Tamborra, *Neutrino quantum kinetics in two spatial dimensions*, *JCAP* **11** (2024) 060, [2407.04769].
- [77] B. Dasgupta, A. Mirizzi and M. Sen, *Fast neutrino flavor conversions near the supernova core with realistic flavor-dependent angular distributions*, *JCAP* **02** (2017) 019, [1609.00528].
- [78] S. Abbar and H. Duan, *Fast neutrino flavor conversion: roles of dense matter and spectrum crossing*, *Phys. Rev. D* **98** (2018) 043014, [1712.07013].



- [79] S. Abbar and H. Duan, *Neutrino flavor instabilities in a time-dependent supernova model*, *Phys. Lett. B* **751** (2015) 43–47, [[1509.01538](#)].
- [80] B. Dasgupta and A. Mirizzi, *Temporal Instability Enables Neutrino Flavor Conversions Deep Inside Supernovae*, *Phys. Rev. D* **92** (2015) 125030, [[1509.03171](#)].